IRIS AperTO

UNIVERSITÀ DEGLI STUDI DI TORINO

AperTO - Archivio Istituzionale Open Access dell'Università di Torino

Surface functionalisation of polypropylene hernia-repair meshes by RF-activated plasma polymerisation of acrylic acid and silver nanoparticles

This is the author's manuscript

Original Citation:

Availability:

This version is available http://hdl.handle.net/2318/153360 since 2016-01-11T17:26:08Z

Published version:

DOI:10.1016/j.apsusc.2014.12.050

Terms of use:

Open Access

Anyone can freely access the full text of works made available as "Open Access". Works made available under a Creative Commons license can be used according to the terms and conditions of said license. Use of all other works requires consent of the right holder (author or publisher) if not exempted from copyright protection by the applicable law.

(Article begins on next page)

26 September 2024

UNIVERSITÀ DEGLI STUDI DI TORINO

***This is an author version of the contribution published on**:*
Questa è la versione dell'autore dell'opera:
[Applied Surface Science, 328, 2015, doi:10.1016/j.apsusc.2014.12.050]

The definitive version is available at:
La versione definitiva è disponibile alla URL:
[http://www.sciencedirect.com/science/article/pii/S016943321402738X]

Surface functionalisation of polypropylene hernia-repair meshes by RF-activated plasma polymerisation of acrylic acid and silver nanoparticles

Roberto Nisticò[a,*], Andrea Rosellini[a], Paola Rivolo[b], Maria Giulia Faga[c], Roberta Lamberti[d], Selanna Martorana[d], Micaela Castellino[e], Alessandro Virga[b], Pietro Mandracci[b], Mery Malandrino[a], Giuliana Magnacca[a]

[a] University of Torino, Department of Chemistry and NIS Research Centre, Via P. Giuria 7, 10125 Torino, Italy
[b] Politecnico di Torino, Dipartimento di Scienza Applicata e Tecnologia, C.so Duca degli Abruzzi 24, 10129 Torino, Italy
[c] CNR-IMAMOTER, Strada delle Cacce 73, 10135 Torino, Italy
[d] Herniamesh S.r.l., Via F.lli Meliga 1/C, 10034 Chivasso, Italy
[e] Center for Space Human Robotics, Istituto Italiano di Tecnologia, Corso Trento 21, 10129 Torino, Italy
* corresponding author. E-mail: roberto.nistico@unito.it, Ph. +39-011-6707533, Fax: +39-011-6707855

Abstract

Hernia diseases are among the most common and diffuse causes of surgical interventions. Unfortunately, still nowadays there are different phenomena which can cause the hernioplasty failure, for instance post-operative prostheses displacements and proliferation of bacteria in the surgical site. In order to limit these problems, commercial polypropylene (PP) and polypropylene/Teflon (PP/PTFE) bi-material meshes were surface functionalised to confer adhesive properties (and therefore reduce undesired displacements)using polyacrylic acid synthesized by plasma polymerisation (PPAA). A broad physico-chemical and morphological characterisation was carried out and adhesion properties were investigated by means of atomic force microscopy (AFM) used in force/distance (F/D) mode. Once biomedical devices surface was functionalised by PPAA coating, metallic silver nanoparticles (AgNPs) with antimicrobial properties were synthesised and loaded onto the polymeric prostheses. The effect of the PPAA, containing carboxylic functionalities, adhesive coating towards AgNPs loading capacity was verified by means of X-ray photo-electron spectroscopy (XPS). Preliminary measurement of the Ag loaded amount and release in water were also investigated via inductively coupled plasma atomic emission spectroscopy (ICP-AES). Promising results were obtained for the functionalised biomaterials, encouraging future *in vitro* and *in vivo* tests.

Keywords: Hernia-repair biomaterials; Plasma polymerization; Polypropylene fibers; Silver nanoparticles; Surface coating.

1. Introduction

Every year, over 20 millions of surgical hernioplasty interventions of various natures (mostly abdominal and inguinal) are performed worldwide [1]. In the United States, this type of clinical operation is the second most performed after the cataract surgery, thus hernia repair is one of the most common cause of surgical operations [2–4].

The classical route for caring hernia diseases is the suturing of damaged body tissues by using polymeric nets, mostly made by polypropylene (PP in the following), polyethylene-terephthalate (PET) or polytetrafluoroethylene (PTFE), depending both on the patients clinical history and surgeons preferences [5,6]. However, even if in the last 60 years health science made important steps forward thanks to novel materials and surgical techniques progresses, still nowadays there is the risk of post-surgery complications [7–9].

As described by Amid [10], causes of hernioplasty failures are at least two.

1) First of all, surgical infections due to implantation of biomaterials which can bring bacteria in the surgical site. In fact, when interstices between mesh fibres are less than 10 μm, bacteria with a diameter less than 1 μm can proliferate every-where, whereas macrophages, too large to enter the infected pores sites, cannot eliminate the infective agents [10]. A possible solution to this steric

problem is the use of polymeric meshes with interstices wider than 10 μm, in order to allow macrophages to enter the site and thus to reduce the infective agents proliferation [11,12]. Unfortunately, sometimes this solution is not sufficient to stop the extension of the infection [8]. In cases like those, an antibacterial coating performing its function directly in the surgical site can be considered [13]. Among other acclaimed antibacterial agents, silver nanoparticles (AgNPs in the following) can develop their activity against bacteria, viruses and eukaryotes micro-organisms when prepared with particles ranging from 1 to 100 nm of diameter [14–18].

2) The second complication considered is due to the shrinking of the prosthesis. In fact, after implantation, meshes contract, inducing the collapse of the anchoring sutures of the prosthesis through the hernia defect margin, leading to hernia disease recurrence [10]. Drainage and utilisation of meshes with dimensions extending several centimetres beyond the margins of the tissue defect guarantee a sufficient coverage and provide adequate contact between the biomaterial and the body tissue, together with the use of glue [19]. These are the solutions up-to-now adopted, but the production of adhesive meshes could significantly simplify the positioning of the prostheses: this is an issue which is still a challenge.

Concerning the specific field of intraperitoneal surgery, a further undesirable effect carried out by macroporous non-continuous prostheses, is the risk of adherences to the viscera. To overcome the problem, bi-material double-layered patches with the parietal side made by a classical hernia-repair net (i.e. PP) and the visceral side made by expanded-PTFE hydrophobic foil able in minimizing the adherences to bowels are manufactured [20–22].

One of the best chances of solving some of the most common questions still opened and described above, is the surface treatment of the prostheses. Among others, plasma treatments [23–25] have recently gained much attention, thanks to their ability to induce modifications only at the surface level without altering the intrinsic physico-chemical and mechanical properties of the prosthetic material [26]. Moreover, by using plasma treatments the coating layer concerns the single fibre of the mesh, allowing to maintain the open porosity necessary for optimal tissue infiltration, thus for proper mesh integration in the biological tissue.

Also plasma polymerisation processes are gaining increasing interest in the formation of thin coatings. The technique bases on transformation reactions between low molecular weight chemical species (monomers or organic precursors) into high molecular weight species (macromolecules or polymeric coatings) taking advantage of the extremely highly reactive environment induced by the plasma phase [27]. Monomer molecules are activated in the plasma and collide toward the material surface, leading to: dissociation at the interface of chemical bonds, etching of the material surface and chemical reactions between surface active sites thus generated and plasma reactive species (mostly monomers). This process is complicated by the fact that, together with monomers polymerisation, surface ablation occurs too [28]. Thus, this implies that reactive species in the plasma phase do not come only from monomers, but also from species generated by the ablation of the already deposited coating. The balance between ablation and polymerisation is controlled by operating parameters, such as gas flow rate, power applied, pressure in the reaction chamber and other characteristics of the apparatus [29]. Therefore, the polymerisation induced by plasma reactive species is completelyd ifferent from traditional processes involving ions and radicals because of different mechanisms regulating the chemical reactions: polymers obtained by plasma polymerisation present differentp hysico-chemical behaviours when compared with those obtained by classical methods [30].

The main advantages concerning coatings produced via plasma-polymerisation are: the possibility to obtain a homogeneous layer with specific chemical functional groups, the control of the coating thickness (from few nanometers to several microns) and the possibility to induce physico-chemical modifications at the surface of the material without altering its bulky properties [31,32].

The technique was successfully used to functionalise polymeric materials with plasma-deposited poly-(acrylic-acid) (PPAA) layers for biodiagnostics purposes [33], exploiting –COOH groups in covalent binding of c-DNA probes. Moreover, carboxylic species, present in PPAA, are particularly

interesting in medical applications since negatively charged groups, in specific buffer solutions, at the surface stimulates cells adhesion in a non-specific manner [34–37].Therefore, PPAA can be studied as coating for developing adhesive materials.
Adhesion properties of materials can be verified by scrolling the AFM tip perpendicularly to the sample surface by fixing the loading/unloading speed toward the surface contact point and subsequently lifting up the tip. During the entire measurement cycle, the corresponding tip deflection values are acquired. The data collected show a force/distance curve and the collected graphics provide information about the interaction between the probe tip and the material surface.
The adhesion forces are expressed by the difference between the minimum value of the curve where contact occurs (jump to contact) and the horizontal segment which represents the moment when the tip is detached from the sample surface [38].
Taking into account all the considerations above reported, aim of this work is the preparation and physico-chemical characterisation of commercial PP and PP/ePTFE hernia-repair meshes with adhesive (induced by PPAA coating) and antibacterial (carried out by Ag nanoparticles) properties.

2. Experimental

2.1 Biomedical devices and reagents

Monofilament PP and composite bi-material PP/ePTFE meshes for surgical applications were provided by Herniamesh® S.r.l.(Chivasso, Italy). Lightweight (ca. 30 g m^{-2}) PP flat rectangular meshes (PM in the main text) probes were 6 cm × 11 cm, with 0.32 ± 10% mm of thickness, and fibres diameter of 80 ± 10% μm. Bi-material PP/ePTFE oval meshes were 11 cm × 14 cm, with 0.55 ± 10% mm of total thickness with ePTFE side of 0.06 ± 0.01-mm thick, and PP fibres diameter of 120 ± 10% and of 180 ± 10% μm. Each side of the bi-material mesh was analysed separately. In the text AM stands for the PP side, BM for the ePTFE side.
Other reagents used are: silver nitrate ($AgNO_3$from Carlo-Erba, purity 99.8%, CAS 7761-88-8), trisodium citrate dihydrate($Na_3C_6H_5O_7{\cdot}2H_2O$ from E. Merck, purity 99%, CAS 6132-04-3), acrylic acid monomer ($CH_2CH(COOH)$ from Sigma Aldrich, purity 99%, CAS 79-10-7), Toluidine Blue O or TBO ($C_{15}H_{16}ClN_3S$ from Sigma, Technical Grade purity, CAS 92-31-9), sodium hydroxide (NaOH from Fluka, purity 97%, CAS 1310-73-2), nitric acid ($HNO_3$from Sigma Aldrich, purity 70%, CAS 7697-37-2), hydrochloric acid (HCl concentrated solution from Fluka Chemika, CAS 7647-01-0) and acetic acid (CH_3COOH from Aldrich, purity 99.7%, CAS 64-19-7).

2.2 Plasma polymerisation apparatus and treatment conditions

Plasma-polymerised poly-(acrylic-acid) (PPAA) thin film deposition was performed in a plasma enhanced CVD reactor (chamber base pressure = 3.7 Pa; RF = 13.56 MHz) equipped with a delivery frame suitable to inject vapours coming from liquid reactants (monomer precursors). The reactor is a cylindrical closed chamber (320 mm wide and 200 mm height) made by stainless steel and argon was selected as gas-carrier in order to sustain plasma discharge, for all experiments.
The complete treatment consists of a two-steps process: (i) the surface etching by continuous Ar plasma (for cleaning the fibres surface and promoting the adhesion of the PPAA coating); (ii) AA polymerisation by pulsed plasma discharge.
Surface etching step was performed by sending an Ar gas(flow = 20 sccm), applying a discharge RF power of 50 W, for 5 min at a total pressure of 30.7 Pa.
Polymerisation was performed by sending acrylic acid vapours(flow = 3 sccm) diluted in Ar (flow = 20 sccm) by a pulsed plasma discharge, applying a discharge RF power of 200 W, a duty cycle of 10% (on time = 10 ms, off time = 90 ms) for 10 min at a total pressure of 19.3 Pa.
Each PPAA-functionalised sample has been soaked in deionized water Milli-Q grade (dH_2O) for 30 min under oscillating shaking in order to remove unstable surface oligomers formed at the end of the plasma process [33]. The expected thickness of PPAA layer for the experimental conditions used is of ca. 100 ± 10 nm, measured on a flat surface.

2.3 TBO titration and carboxylic functionality density quantification

The amount of –COOH functionalities of PPAA was tested with Toluidine Blue O (TBO). This dye is normally used to evaluate the surface density of carboxylic groups on a surface by means of colorimetric titration of the recovered solution. The amino group contained in TBO molecule reacts with a surface carboxylic group according to a 1:1 ratio [39]. PPAA-functionalised samples were contacted with 3 mL of 0.5 mM TBO aqueous solution (pH 10) at 37◦C for 5 h in the dark. To remove the unreacted dye, meshes were rinsed with copious amount of 0.1 mM NaOH solution. Afterwards, samples were rinsed in 1.5 ml of 50% (v/v) acetic acid solution and oscillating shacked for 10 min, in order to complete release the TBO linked to the carboxylic functional groups. Colorimetric evaluation of TBO (and consequently of carboxylic groups) was performed by using a double beam UV–vis-NIR Varian Cary 5000 spectrophotometer, in transmission mode. All the spectra were obtained by using a quartz cuvette and monitoring λ_{max}= 633 nm. A solution of 50% (v/v) acetic acid was used as reference background.
The evaluation of carboxylic functionalities density (in terms of groups $cm^{-2}$of mesh) was performed through the Lambert–Beer law and applying the Avogadro constant ($6.022 \times 10^{23}\,mol^{-1}$), on the basis of an external calibration with TBO solutions (at known concentrations and volumes) and a multiplex replication of experimental values. Finally, –COOH amount was normalized for the geometric surface of mesh samples.

2.4 Synthesis and loading of AgNPs

AgNPs solutions were prepared by the method already described by Turkevich et al. [40,41]. Briefly, 100 mL of 1 mM $AgNO_3$aqueoussolution is heated up to 90°C under magnetic stirring, 1 mL of 0.3 M trisodium citrate aqueous solution (pre-heated at 90°C) has been added drop wise to the silver-containing solution. After 12–15 min, the solution turns yellow (thus indicating the formation of AgNPs).After 20 min of reaction time, the AgNPs solution has been cooled down to RT by running water continuing stirring for 1 h.
In the loading procedure, prostheses (both original and plasma-functionalised) were dipped inside the $AgNO_3$solution for 15 min at RT under slow stirring, making sure that PPAA functionalised side was directly in contact with the solution. After that, solutions containing prostheses were heated up to 90°C following the AgNPs synthesis procedure. No modification of PPAA-coating was observed after 90°C thermal treatment carried out for AgNPs synthesis, as expected considering PPAA thermal degradation behaviours reported in the literature [42]. At the end of the process, the functionalised biomedical devices were taken out from the solution and air dried using a rotating apparatus (2 rpm) *ad hoc* realised in order to avoid accumulation of solution on one side of the mesh and to obtain a homogeneous loading.

2.5 Physico-chemical characterisation techniques

Static (sessile drop) water contact angle (WCA) measurements were performed by using OCAH200 (Dataphysics, Instruments GmbH). At RT, 1.5 µL of dH_2O was spotted onto the surfaces and images of the droplets were captured. SCA20 software was used to fit drop profiles through the Young–Laplace method and, indeed, to calculate contact angles between fitted function and baseline. The instrument automatically calculates the contact angle, allowing to roughly estimate the hydrophilic/hydrophobic behaviour of the material surface. At least three drops were dispensed for each sample.
FTIR spectra were recorded in Attenuated Total Reflection mode(diamond cell for single reflection) in a Bruker IFS28 spectrophotometer equipped with Globar source, DTGS detector and working with 128 scans at 4 $cm^{-1}$of resolution in the range 4000–400 cm^{-1}. ATR-FTIR spectra were obtained on single fibres repeating the acquisition for three times.
The adhesion force of the PPAA functionalised biomaterials was evaluated by atomic force microscopy (AFM) [38]. Analyses were performed in air at RT with a Park Systems Instrument, model XE-100. Silicon micro-cantilevers with the reflective side coated with aluminium (force constant 3.0 N m^{-1}, frequency constant 60 kHz)and tetrahedral silicon tip (radius of curvature less

than 8 nm, tip height 20–25 μm, full tip cone angle less than 30°) were used. Probe dimensions were 200 μm length, 40 μm wide and 2 μm thick. AFM investigations were carried out using the force/distance (F/D) mode to measure adhesion forces between the AFM probe and the adhesive PPAA coating. The loading/unloading speed was 0.3 μm–s^{-1}. A F/D curve is a plot of the force between the tip and the sample as a function of the Z scanner extension. To calibrate tips force, measurements were done on a glass surface previously cleaned by acetone solution and then heated up in an oven at 100°C for 1 hand cooled down to RT. All adhesion force measurements were performed more than 10 times and average values were reported with the standard deviations.

UV–vis spectra of AgNPs colloidal solution were recorded by UV–vis Varian Cary 300 Scans with scan interval of 1 nm.

UV–vis spectra of AgNPs loaded prostheses were recorded in diffuse reflection mode (integrating sphere and $BaSO_4$ paint as reference) in a UV–vis-NIR Varian Cary 5000 in the range 200–700 nm and scan interval of 1 nm.

Field emission scanning electron microscopy (FESEM) was used to analyse the functionalised meshes surface. Micrographs were obtained by using a FESEM SUPRA 40 ZEISS microscope equipped with a W source using an accelerating voltage of 1 kV.

High resolution transmission electron microscopy (HRTEM) was used to evaluate the AgNPs morphology. Micrographs were obtained by a JEOL 3010 instrument (300 kV) equipped with a LaB_6 filament coupled with energy dispersive X-ray spectroscopy (EDS). For the specimen preparation few drops of AgNPs colloidal solution were poured on holed carbon coated copper grids and left drying overnight. The pattern of diffraction of such samples was investigated by analysing the selected area electron diffraction (SAED) directly performed inside the TEM.

X-ray photoelectron spectroscopy (XPS) studies were carried out by a Versa Probe 5000 from PHI electronics, using Summitas software. Spectra were analysed using Fityk software. Al Kα radiation (1486.6 eV), having a beam diameter of 100 μm, was used as X-rays source. C1s, O1s, S2p and Ag3d signals were analysed. All core-level peak energies were referenced to C1s peak at 284.5 eV assignable to the surface accumulated adventitious carbon.

Ag determination was performed with a Perkin Elmer Optima7000 DV Model Inductively Coupled Plasma Atomic Emission Spectrometer (ICP-AES). The instrument is equipped with an Echelle monochromator, a cyclonic spray chamber, and a PTFE Mira Mist nebulizer. The instrumental conditions used were: plasma power 1.3 kW; torch temperature between 7500 and 8000 K; Ar sampling flow 15 L min^{-1}. The Ag emission line considered was 328.068 nm. The overall Ag amount loaded on prostheses was measured by ICP-AES after *aqua regia* treatment at 90°C for 24 h. In particular, the release test was made by soaking AgNPs loaded on PPAA-functionalised PM meshes (3 cm × 3 cm) into 50 mL of bi-distilled water for 2 weeks under magnetic stirring. After that the solution thus obtained was acidified with 100 μL of HNO_3 before being analysed. External calibration has been made and a weakly acid HNO_3 aqueous solution was used as reference background. AgNPs loading amount on PM before and after the release test in water was made by prostheses preliminary digestion in 120 mL of *aqua regia* for 24 h. Even if the complete polymer dissolution has not been reached, it is reasonable to assume that silver almost completely passed into solution. Solutions thus obtained were diluted 1:10 with distilled water. External calibration has been made and a 1:10 diluted *aqua regia* solution was used as reference background.

3. Results and discussion

3.1 Plasma polymerisation and surface functionalisation

Immediately after the plasma polymerisation treatment (i.e. 30 min later), PPAA surface wettability/hydrophilicity were evaluated by water contact angle (WCA) measurements. Fig. 1 highlights the reduction of contact angle values, which corresponds to the increase of surface hydrophilicity, for functionalised PM samples from 139 ± 1° for non-treated fibres to 74 ± 1° for functionalized ones.

WCA measurements were also carried out on the fibres backside, the one not directly exposed to acrylic acid vapours during the plasma polymerisation step. The data observed confirmed that even the prostheses back sides show an increment, although more limited, of the surface wettability, showing a WCA of 88 ± 2°. The same trends were obtained for AM and BM samples, although a comparison between the WCA absolute values relative to PP fibres (PM and AM) is almost unreliable because the geometry of the samples complicates the contact angle measurements. The samples hydrophilicity change should depend on carboxylic functionalities carried by PPAA, which can be varied by modifying the experimental condition of the plasma polymerisation.

The presence of PPAA can be estimated by IR spectroscopic measurements. Infrared spectra of PM fibres before and after the PPAA-functionalisation, together with the spectrum of a commercial PAA material, are reported in Fig. 2.

The PM fibres, after functionalisation, show the PAA absorption signals, in particular at 3500–3000 cm^{-1}, due to the hydroxyl –OH single bond stretching, at 1710 $cm^{-}1$, due to the carbonyl C=O double bond stretching, and a broad signal at 1250 cm^{-1}, due to the carboxyl C-O single bond stretching [33]. Analogous results were obtained for AM samples (Fig. 2) and BM samples (Fig. SM-1), even if in the latter case the intensity of PPAA signals was very low. In this case, no PPAA signals were detected on BM back side, although WCA indicated an increase of hydrophilicity. The reason of this odd behaviour can be explained considering the entire plasma treatment procedure. In fact, the first step of plasma treatment consists in the surface etching of the fibres carried out by a continuous Ar plasma discharge. This treatment is very effective and causes the modification of the whole polymeric fibre (front and back sides) which becomes more hydrophilic. When the plasma-polymerisation occurs, only the portion of fibres directly exposed to AA species under plasma discharge is coated by the resulting PPAA coating. Formation of PPAA coating on fibres back side is not induced [43–45].

The carboxylic functionality density on the functionalised prostheses surface was determined by means of TBO colorimetric titrations (external calibration curve reported in Fig. SM-2). The procedure was applied to both PM and PP/ePTFE samples as well asPPAA functionalised prostheses.

The average values of carboxyl functionality density for PM and PP/ePTFE samples are reported in Table 1. The titration gave negative results (i.e. complete absence of carboxyl groups) for non-treated PM meshes, whereas both PPAA functionalised PM and PP/ePTFE samples presented a high carboxylic functionality density. The value obtained for PM meshes is 1 order of magnitude lower than that relative to bi-material ones (AM samples). Thus, in principle, the functionalisation of bi-material PP/ePTFE meshes is favoured with respect to the PM devices, due to both the presence of voids among PP fibres (calculated geometrical area takes in account both fibres and interstices) and to the fabrication characteristics of the bi-material meshes that ensure a continuity between the PP and the ePTFE portions with probable PPAA accumulation at intersection points.

From the morphological point of view, it is not easy to highlight the PPAA surface functionalisation of PM fibres. FESEM analyses allowed to evaluate the morphological behaviours of the meshes. The images are reported in Fig. 3. The morphological evaluation of AM and PM samples does not allow to evidence the PPAA presence, probably for the limited thickness of the coating (ca. 100 ± 20 nm)and for its chemical nature, very close to that of the PP substrate. Otherwise, the presence of PPAA coating seems to be visible only on BM samples: the porosity of ePTFE material is not visible after functionalisation and the surface appears smooth and without irregularities.

3.2 AFM force/distance measurements: adhesion force evaluation

Adhesive properties were evaluated only for PM samples before and after PAA functionalisation by means of AFM F/D measurements. This technique allows the measurements of surface weak forces and provides information on surface energetic behaviours [38].

The curves F/D are reported in Fig. 4 and it is possible to evidence the difference between the two samples. The adhesion force exerted by PPAA functionalised mesh toward the silicon tip probe is

approximately two times higher (25.2 ± 2.9 nN) than the reference PM material (13.6 ± 4.8 nN). This suggests that PPAA coated on PP meshes actually induces adhesive properties to the device. Further studies carried out on epidermises tissue (i.e. ASTM F2255-03"Standard Test Method for Strength Properties of Tissue Adhesives in Lap-Shear by Tension Loading" [46]) are necessary to confirm the preliminary results.

3.3 Synthesis and loading of AgNPs

The Turkevich synthesis [40] deals with the formation of AgNPs colloidal suspension using trisodium citrate as reducing agent and stabilizer. Moreover, AgNPs physico-chemical parameters (i.e. shape and size) strongly depend on the reaction parameters, particularly on the stabilizer concentration, reaction time and temperature.

Fig. 5 reports the UV–vis spectra of the AgNPs colloidal solution. The registered band is due to the surface phenomenon of plasmonic resonance, which indicates the presence of zero-valence metallic particles of nanometric dimensions. The spectrum presents the absorbance maximum at 425 nm, a characteristic value for AgNPs [47]. The enlarged band shape suggests a wide dimensional distribution of the produced AgNPs. Morphologic evaluations (reported in Fig. 6) confirm the spectroscopic evidence. In particular, it is possible to register the presence of both isolated nanoparticles together with AgNPs aggregates with variable dimensions. Single nanoparticles show size from few nanometers up to 20–25 nm and the majority of AgNPs synthesised presents an irregular spherical shape. At high magnification, it was possible to appreciate the poly-crystalline nature of these particles given by coalescence of primary ones [48]. The shape of the particles observed is very similar to the one described by Personick et al. [49]. The analysis of the fringe patterns reveals the presence of hexagonal Ag (2.20Å is the preferential d_{hkl} observed, relative to plane (112), reference pattern 00-041-1402).

AgNPs were synthesized following the Turkevich procedure in the presence of prosthetic devices. The aspect of the PPAA functionalised meshes before and after AgNPs synthesis indicates that the loading occurred (see Fig. SM-4 reported in the Supplementary Material) since a characteristic yellowish colour, typical of the plasmonic resonance phenomenon due to AgNPs, is developed after the synthesis. The same devices without PPAA coating do not present a visible colour change. UV-vis spectra carried out in diffuse reflection mode on AgNPs loaded PM prostheses were registered in Fig. 7. As suggested by the visual exam, PPAA functionalised prostheses present the signal related to AgNPs at 415 nm (i.e. a band position very close to that observed for AgNPs colloidal solution reported in Fig. 5), whereas no signals are visible for the not-functionalised PM fibres. Analogous results, not reported for the sake of brevity, were obtained for bi-material prostheses.

Indeed, PPAA carboxyl groups (negatively charged) are able to interact with the Ag^+ species present in the solution and immobilised them. The subsequent reduction reaction would form AgNPs anchored at the PPAA surface. The same trend is observed for bi-material devices.

PP surfaces were analysed by X-ray photoelectron spectroscopy in order to characterise the composition of the outermost layer of the fibres. XPS spectra of AgNPs loaded on PM are reported in Fig. 8, together with the spectra obtained for PPAA-coated PM fibres and PPAA-coated PP/ePTFE meshes. The most important ranges are reported in Fig. 8, namely C1s and Ag3d. XPS spectra of AgNPs loaded PM fibres evidences a weak contribution due to metallic silver [50,51] (0.6 atomic % of the examined layer), probably because the not-treated PM fibres do not show affinity with Ag^+ precursor, as demonstrated by the very low amount of oxygenated (i.e. reactive) surface species in the C1s signal (only 5 atomic % of the C1ssignal is assignable to C–O species [26]). Indeed, the small amount of oxygenated species seems to be formed during Turkevich synthesis since no oxidative processes were carried out on PM fibres before AgNPs formation.

On the other hand, the analysis of the meshes coated by PPAA should be representative only of the PPAA layer since the depth of the analysis does not overcome the thickness of the PPAA layer which is supposed to be ca. 100 nm. In this case many oxygenated C species are visible (15 atomic % of C-O and 8 atomic % of HO-C=O of the C1s signal [26]) which can be assigned to polyacrylic

acid. The amount of metallic Ag revealed is 8.5 atomic % of the examined layer, which corresponds to an amount ten times higher with respect to the previous sample. The results suggest that the plasma PPAA coating treatment induced the formation of functional groups able to favour the loading of metallic AgNPs. Impurity presence (mostly SO_4^{2-}) was registered in all samples, probably derived from Ag precursor.
The analysis of PPAA functionalised bi-material PP/ePTFE samples indicates the presence of 3.0 atomic % of Ag, notwithstanding the verified higher surface density of carboxylic functionalities. Thus, a mechanism of promotion of Ag reduction involving the -COOH functionality cannot be invoked. The higher Ag % revealed in PM samples does not depend on the higher extent of PPAA coating and can only be ascribed to the more structured morphology that can favour higher clustering of AgNPs and inhomogeneity on XPS investigation area.
The Ag-functionalised PM meshes (i.e. the meshes with the highest Ag loading) were analysed by means of ICP-AES technique for determining the amount of Ag loaded on the meshes and the amount of Ag released in water after 15 days of soaking.
Results of these preliminary tests are reported in Table 2. Considering the PP mesh grammage (30 g m^{-2}), the AgNPs loading valuated after acid attack and following ICP-AES analysis corresponds to 1.1 wt.%. Only ca. 0.1 wt.% is released after 15 days of water soaking, as indicated by ICP-AES analysis on soaking solution. The difference of ca. 1.0 wt.% corresponds to the amount of AgNPs remained on meshes after soaking procedure. The ICP-AES analysis carried out on the mesh after soaking and after acid attack brings a value of ca. 0.9 wt.% of AgNPs still interacting with the device, in good agreement with the other measurements. The small difference observed could be ascribed to many factors, among others the digestion methodology adopted that needs to be optimized. More accurate and detailed analyses will be object of further studies. Notwithstanding, the preliminary test indicates that at least 81 wt.% of silver loaded on PM mesh remains onto the biomedical device surface after two weeks in water. This implies that silver is not released completely from the mesh and can continue carryout its antimicrobial action directly in situ avoiding the biofilms formation in the surgical site.

4. Conclusions

An adhesive PPAA coating obtained via plasma polymerization of acrylic acid vapour has been realised. A broad physico-chemical characterisation has been done, confirming the presence of the PPAA coating and assessing the amount of carboxyl functionality available. Characterisation results highlight the deposition process reproducibility. AFM F/D studies confirmed the adhesion capacity of PPAA functionalised devices.
The surface modification was exploited also for loading AgNPs with well-known antimicrobial capacities and the effect of PPAA-coating in enhancing the AgNPs loading was evidenced.
Preliminary studies of AgNPs release in water showed that the majority of AgNPs remains on the mesh surface and this implies that they can assess their antimicrobial activity with two different actions: immediately after the surgical operation the silver released in solution can exert the antimicrobial action in the aqueous environment nearby the surgical site, whereas the silver remained at the biomedical device surface can reduce the formation and/or the adhesion of bacteria biofilms onto the prostheses interface. This opportunity needs to be investigated in future by *in vitro* and *in vivo* tests.

5. Acknowledgements

The authors would like to thank Dr. Pierangiola Bracco for suggestions and comments, Mrs. Federica Franconieri together with Dr. Ettore Bernardi for technical assistance and Mr. Giuseppe Salerno (from Givoletto, Italy) for the realisation of the rotating dryer.

References

[1] A. Kingsnorth, Introduction to current practice of adult hernia repair, World J. Surg. 29 (2005) 1044–1045.
[2] I.M. Rutkow, Surgical operations in the United States. Then (1983) and now(1994), Arch. Surg. 132 (1997) 983–990.
[3] A. Kingsnorth, K. LeBlanc, Hernias: Inguinal and incisional, Lancet 362 (2003) 1561–1571.
[4] M.S. Sajid, L. Kalra, U. Parampalli, P.S. Sains, M.K. Baig, A systematic review and meta-analysis evaluating the effectiveness of lightweight mesh against heavyweight mesh in influencing the incidence of chronic groin pain following laparoscopic inguinal hernia repair, Am. J. Surg. 205 (2013) 726–736.
[5] R.C. Read, The contributions of Usher and others to the elimination of tension from groin herniorrhaphy, Hernia 9 (2005) 208–211.
[6] A. Coda, R. Lamberti, S. Martorana, Classification of prosthetics used in hernia repair based on weight and biomaterial, Hernia 16 (2012) 9–20.
[7] J.W.A. Burger, R.W. Luijendijk, W.C.J. Hop, J.A. Halm, E.F.F. Verdaasdonk, J. Jeekel,Long-term follow-up of a randomized controlled trial of suture versus mesh repair of incisional hernia, Ann. Surg. 240 (2004) 578–585.
[8] P.K. Amid, A.G. Shulman, I.L. Lichtenstein, M. Hakakha, The goal of modern hernia surgery. How to achieve them: open or laparoscopic repair? Probl. Gen.Surg. 12 (1995) 165–171.
[9] A.F. Engelsman, H.C. van der Mei, R.J. Ploeg, H.J. Busscher, The phenomenon of infection with abdominal wall reconstruction, Biomaterials 28 (2007) 2314–2327.
[10] P.K. Amid, Classification of biomaterials and their related complications in abdominal wall hernia surgery, Hernia 1 (1997) 15–21.
[11] R.G. Molloy, K.T. Moan, R.P. Waldron, M.P. Brady, W.O. Kirwan, Massive incisional hernias: abdominal wall replacement with Marlex mesh, Br. J. Surg. 78(1991) 242–244.
[12] D.L. Sanders, A.N. Kingsnorth, J. Lambie, P. Bond, R. Moate, J.A. Steer, An experimental study exploring the relationship between the size of bacterial inoculum and bacterial adherence to prosthetic mesh, Surg. Endosc. 27 (2013) 978–985.
[13] P. Avetta, R. Nisticò, M.G. Faga, D. D'Angelo, E. Aimo Boot, R. Lamberti, S. Martorana, P. Calza, D. Fabbri, G. Magnacca, Hernia-repair prosthetic devices functionalised with chitosan and ciprofloxacin coating: controlled release and antibacterial activity, J. Mater. Chem. B 2 (2014) 5287–5294.
[14] M.M. Rai, A. Yadav, A. Gade, Silver nanoparticles as a new generation of antimicrobials, Biotechnol. Adv. 27 (2009) 76–83.
[15] K. Virender, R.A. Sharma, Y.L. Yngard, Silver nanoparticles: green synthesis and their antimicrobial activities, Adv. Colloid Interface Sci. 145 (2009) 83–96.
[16] S. Chernousova, M. Epple, Silver as antibacterial agent: ion, nanoparticle, and metal, Angew. Chem. Int. Ed. 52 (2013) 1636–1653.
[17] V. Virendra Kumar, C. Jolivalt, J. Pulpytel, R. Jafari, F. Arefi-Khonsari, Development of silver nanoparticle loaded antibacterial polymer mesh using plasma polymerization process, J. Biomed. Mater. Res. A 101 (2013) 1121–1132.
[18] J.J. Wu, G.J. Lee, Y.S. Chen, T.L. Hu, The synthesis of nano-silver/polypropylene plastics for antibacterial application, Curr. Appl. Phys. 12 (2012) 89–95.
[19] G. Champault, C. Polliand, F. Dufour, M. Ziol, L. Behr, A "self-adhering" prosthesis for hernia repair: experimental study, Hernia 13 (2009) 49–52.
[20] G.M. Eid, J.M. Prince, S.G. Mattar, G. Hamad, S. Ikrammudin, P.R. Schauer, Medium-term follow-up confirms the safety and durability of laparoscopic ventral hernia repair with PTFE, Surgery 134 (2003) 599–604.
[21] Y.W. Novitsky, A.G. Harrell, J.A. Cristiano, B.L. Paton, H.J. Norton, R.D. Peindl, K.W. Kercher, B.T. Heniford, Comparative evaluation of adhesion formation, strength of ingrowth, and textile properties of prosthetic meshes after long-term intra-abdominal implantation in a rabbit, J. Surg. Res. 140 (2007) 6–11.

[22] W.S. Cobb, J.B. Harris, J.S. Lokey, E.S. McGill, K.L. Klove, Incisional herniorrhaphy with intraperitoneal composite mesh: a report of 95 cases, Am. Surg. 69 (2003) 784–787.
[23] N.Y. Cui, N.M.D. Brown, Modification of the surface properties of a polypropylene (PP) film using an air dielectric barrier discharge plasma, Appl. Surf. Sci.189 (2002) 31–38.
[24] J. Lai, B. Sunderland, J. Xue, S. Yan, W. Zhao, M. Folkard, B.D. Michael, Y. Wang, Study on hydrophilicity of polymer surfaces improved by plasma treatment, Appl. Surf. Sci. 252 (2006) 3375–3379.
[25] R. Nisticò, M.G. Faga, G. Gautier, G. Magnacca, D. D'Angelo, E. Ciancio, G. Piacenza, R. Lamberti, S. Martorana, Physico-chemical characterization of functionalized polypropylenic fibers for prosthetic applications, Appl. Surf. Sci. 258(2012) 7889–7896.
[26] R. Nisticò, G. Magnacca, M.G. Faga, G. Gautier, D. D'Angelo, E. Ciancio, R. Lamberti, S. Martorana, Effect of atmospheric oxidative plasma treatments on polypropylenic fibers surface: characterization and reaction mechanisms, Appl. Surf. Sci. 279 (2013) 285–292.
[27] R. Forch, Z.H. Zhang, W. Knoll, Soft plasma treated surfaces: tailoring of structure and properties for biomaterial applications, Plasma Process. Polym. 2 (2005) 351–372.
[28] H. Yasuda, New insights into aging phenomena from plasma chemistry, Nucl. Instrum. Meth. Phys. Res. A 515 (2003) 15–30.
[29] H. Yasuda, Plasma Polymerization, Academic Press Inc., Orlando (Florida, USA), 1985.
[30] F.F. Shi, Recent advances in polymer thin films prepared by plasma polymerization. Synthesis, structural characterization, properties and applications, Surf. Coat. Technol. 82 (1996) 1–15.
[31] J. Friedrich, G. Kühn, R. Mix, A. Fritz, A. Schonhals, Polymer surface modification with monofunctional groups of variable types and densities, J. Adhesion Sci. Technol. 17 (2003) 1591–1617.
[32] E.M. Liston, L. Martinu, M.R. Wertheimer, Plasma surface modification of polymers for improved adhesion: a critical review, J. Adhesion Sci. Technol. 7 (1993) 1091–1127.
[33] S. Ricciardi, R. Castagna, S.M. Severino, I. Ferrante, F. Frascella, E. Celasco, P. Mandracci, I. Vallini, G. Mantero, C.F. Pirri, P. Rivolo, Surface functionalization by poly-acrylic acid plasma-polymerized films for microarray DNA diagnostics, Surf. Coat. Technol. 207 (2012) 389–399.
[34] K.S. Siow, L. Britcher, S. Kumar, H.J. Griesser, Plasma methods for the generation of chemically reactive surfaces for biomolecule immobilization and cell colonization - a review, Plasma Process. Polym. 3 (2006) 392–418.
[35] M.R. Alexander, T.M. Duc, The chemistry of deposits formed from acrylic acid plasmas, J. Mater. Chem. 8 (1998) 937–943.
[36] J.H. Lee, J.W. Lee, G.S. Khang, H.B. Lee, Interaction of cells on chargeable functional group gradient surfaces, Biomaterials 18 (1997) 351–358.
[37] L. Detomaso, R. Gristina, G.S. Senesi, R. d'Agostino, P. Favia, Stable plasma deposited acrylic acid surfaces for cell culture applications, Biomaterials 26 (2005) 3831–3841.
[38] H.J. Lee, S. Hyun, J.H. Kim, H.J. Lee, D.G. Choi, D.I. Lee, J.H. Jeong, E.S. Lee, Measurement of adhesion force by a symmetric AFM probe for nano-imprint lithography application, J. Adhesion Sci. Technol. 22 (2008) 1379–1386.
[39] J.P. Chen, Y.P. Chiang, Surface modification of non-woven fabric by DC pulsed plasma treatment and graft polymerization with acrylic acid, J. Membr. Sci. 270(2006) 212–220.
[40] J. Turkevich, P.C. Stevenson, J. Hillier, A study of the nucleation and growth processes in the synthesis of colloidal gold, Discuss. Faraday Soc. 11 (1951) 55–75.
[41] L.F. Gorup, E. Longo, E.R. Leite, E.R. Camargo, Moderating effect of ammonia on particle growth and stability of quasi-monodisperse silver nanoparticles synthesized by the Turkevich method, J. Colloid Interface Sci. 360 (2011) 355–358.
[42] S. Dubinsky, G.S. Grader, G.E. Shter, M.S. Silverstein, Thermal degradation of poly(acrylic acid) containing copper nitrate, Polym. Degrad. Stab. 86 (2004) 171–178.
[43] C. Canal, R. Molina, E. Bertran, P. Erra, Wettability, ageing and recovery process of plasma-treated polyamide 6, J. Adhesion Sci. Technol. 18 (2004) 1077–1089.

[44] J. Nakamatsu, L.F. Delgado-Aparicio, R. Da Silva, F. Soberón, Ageing of plasma-treated poly(tetrafluoroethylene) surfaces, J. Adhesion Sci. Technol. 13 (1999) 753–761.
[45] E.T. Kang, K.L. Tan, K. Kato, Y. Uyama, Y. Ikada, Surface modification and functionalization of polytetrafluoroethylene films, Macromolecules 29 (1996) 6872–6879.
[46] ASTM F2255-05, Standard Test Method for Strength Properties of Tissue Adhesives in Lap-Shear by Tension Loading, ASTM International, West Con-shohocken (Pennsylvania, USA), 2005.
[47] Z.S. Pillai, P.V. Kamat, What factors control the size and shape of silver nanoparticles in the citrate ion reduction method? J. Phys. Chem. B 108 (2004) 945–951.
[48] A. Henglein, M. Giersig, Formation of colloidal silver nanoparticles: capping action of citrate, J. Phys. Chem. B 103 (1999) 9533–9539.
[49] M.L. Personick, M.R. Langille, J. Wu, C.A. Mirkin, Synthesis of gold hexagonal bipyramids directed by planar-twinned silver triangular nanoprisms, J. Am. Chem. Soc. 135 (2013) 3800–3803.
[50] X. Ping, M. Wang, G. Xuewu, Surface modification of poly(ethylene terephthalate) (PET) film by gamma-ray induced grafting of poly(acrylic acid) and its application in antibacterial hybrid film, Rad. Phys. Chem. 80 (2011) 567–572.
[51] M. Castellino, V. Stolojan, A. Virga, M. Rovere, K. Cabiale, M.R. Galloni, A. Tagliaferro, Chemico-physical characterisation and in vivo biocompatibility assessment of DLC-coated coronary stents, Anal. Bioanal. Chem. 405 (2013) 321–329.

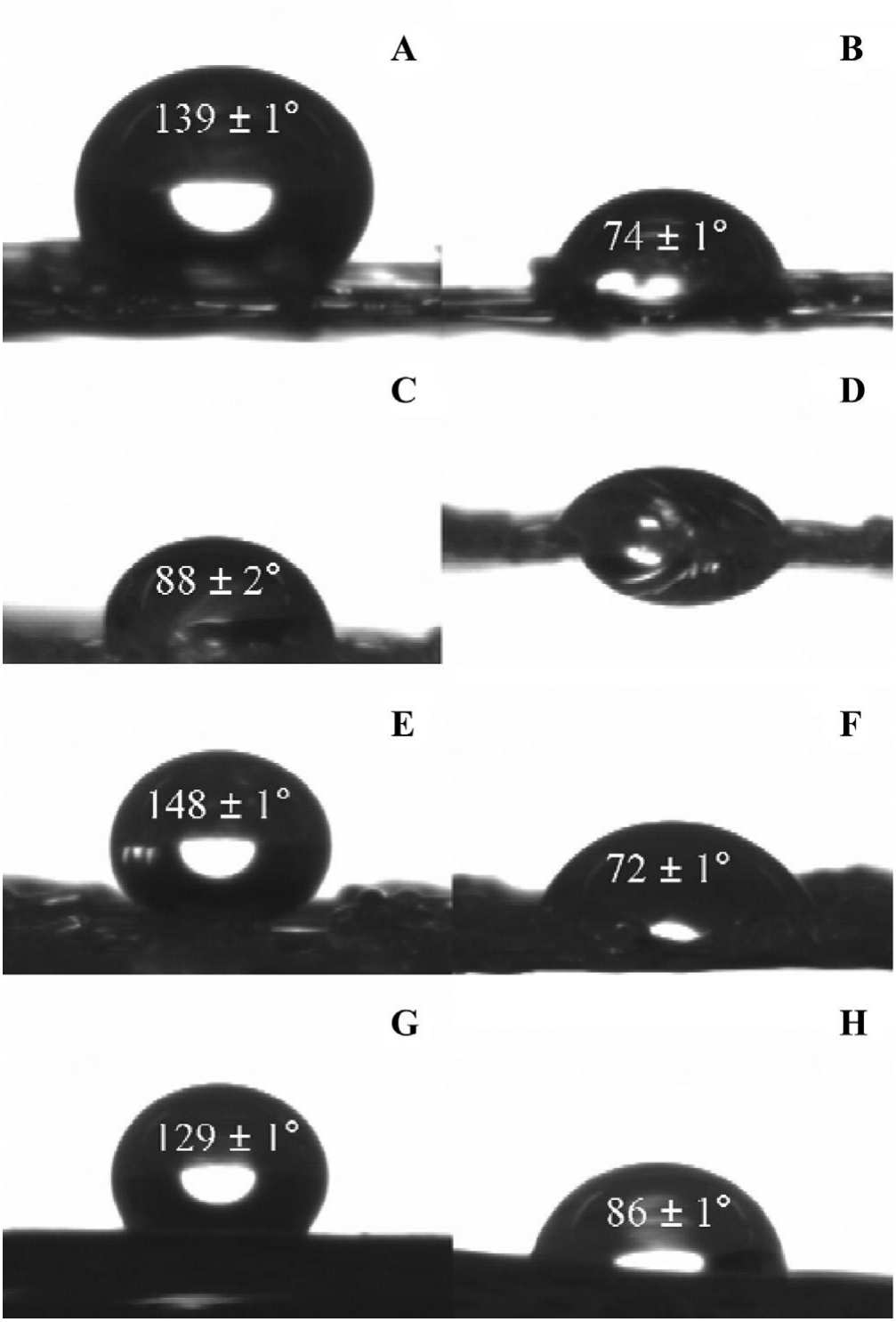

Figure 1. WCA observed for (A) PM fibres, (B) PPAA functionalised PM fibres, (C) PPAA functionalised PM fibres back side, (D) PPAA functionalised PM meshes (the image reports the drop passing through the mesh), (E) AM fibres, (F) PPAA functionalized AM fibres, (G) BM fibres back side and (H) PPAA functionalised BM fibres back side.

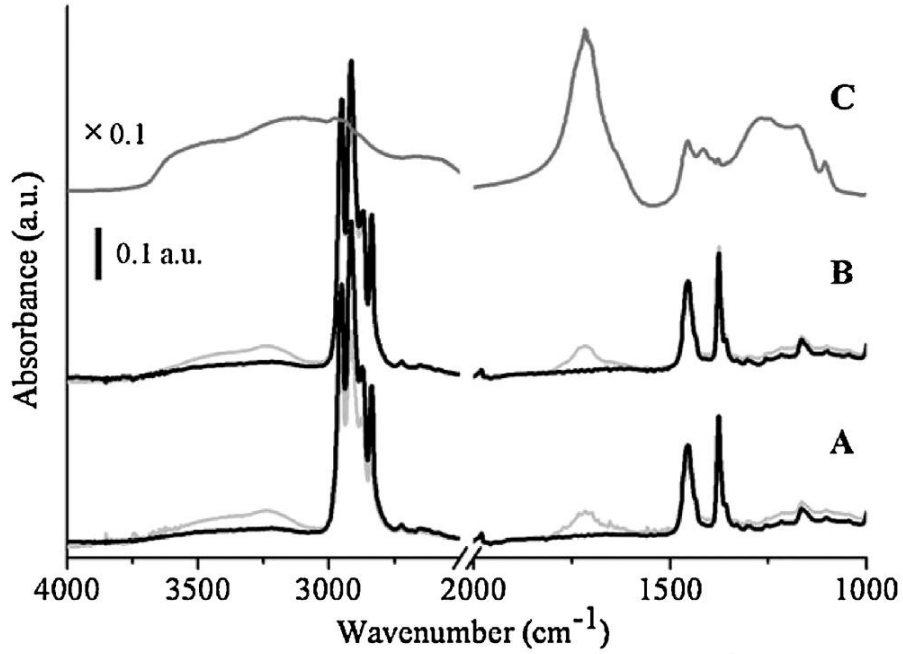

Figure 2. Absorbance IR spectra in the 4000–2500 cm^{-1}range and in the2000–1000 cm^{-1}range of: (A) PM fibres before (black solid line) and after (grey solid line) plasma-induced PPAA coating; (B) AM fibres before (black solid line) and after (grey solid line) plasma-induced PPAA coating; (C) commercial PAA film. Spectra A and B were collected in the ATR mode, whereas spectrum C is collected in transmission mode.

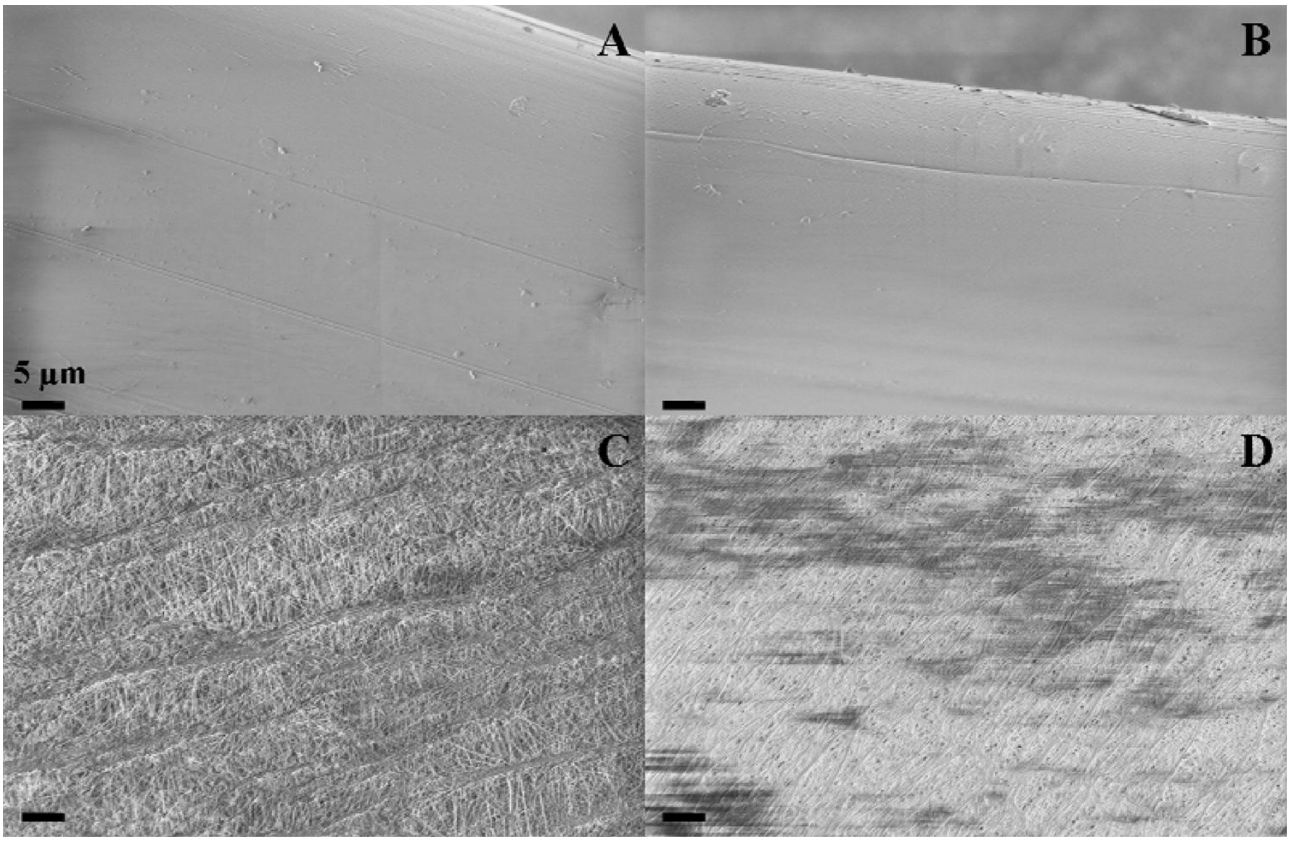

Figure 3. FESEM micrographs of (A) PM fibres and (B) PPAA functionalised PM fibres, (C) BM patch and (D) PPAA functionalised BM patch.

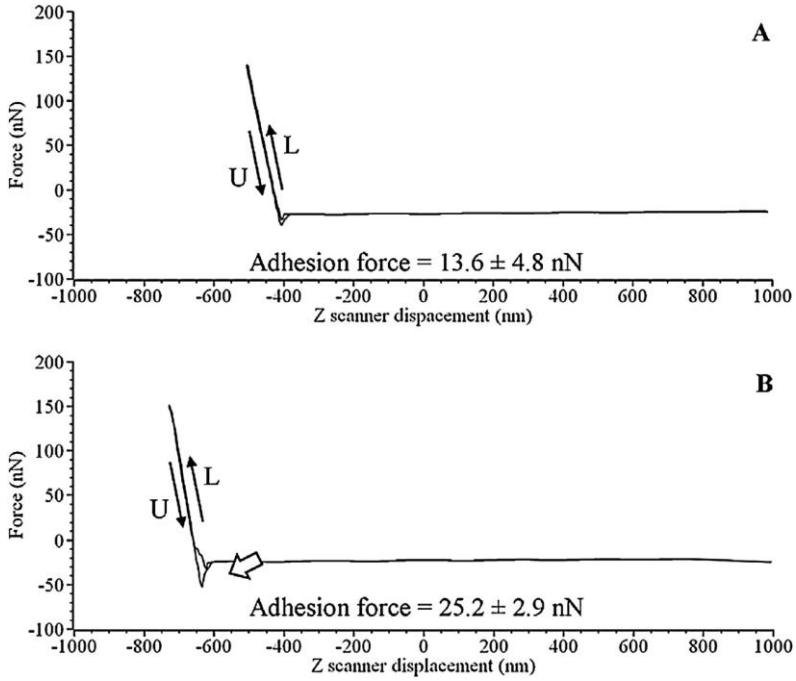

Figure 4. Adhesion force test results on force vs Z scanner displacement curves between silicon tip probe and (A) PM reference material and (B) PPAA functionalised PM material. Black arrows indicate the direction of loading (L) and unloading (U) processes. The white arrow in section B evidences the adhesion force, calculated as the unloading force change at the minimum value of the loading force.

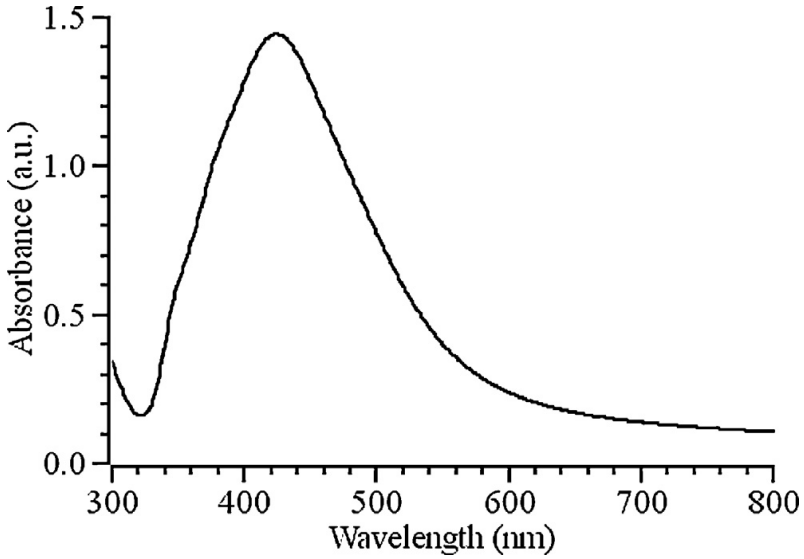

Figure 5. Absorbance UV–vis spectra of AgNPs colloidal solution.

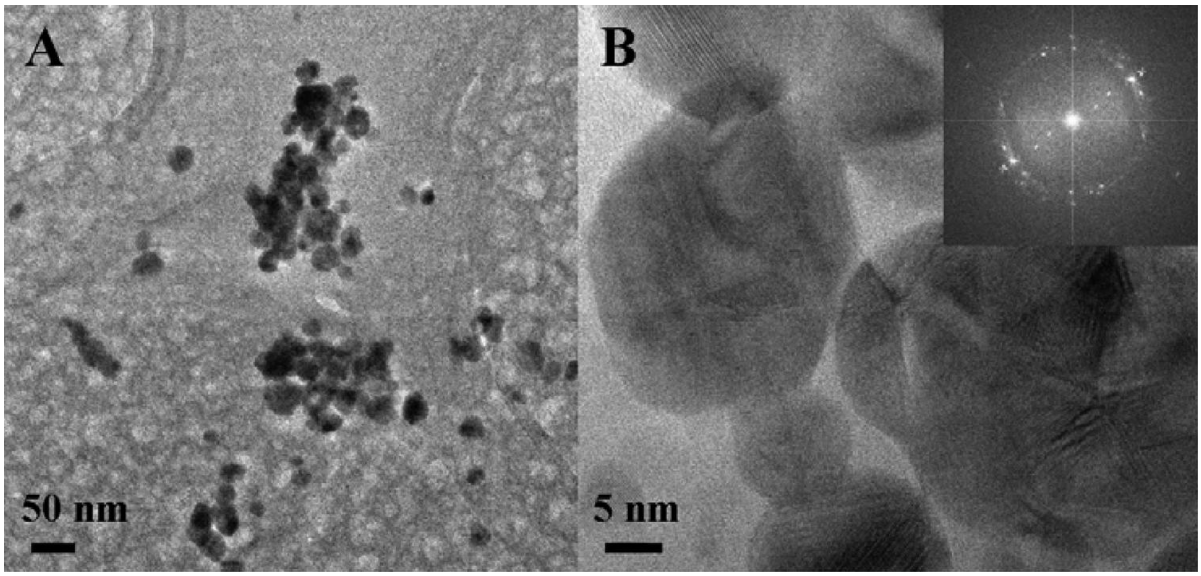

Figure 6. TEM micrographs of AgNPs at low (A) and high (B) magnifications. Inset in section B shows the polycrystalline Ag diffraction pattern.

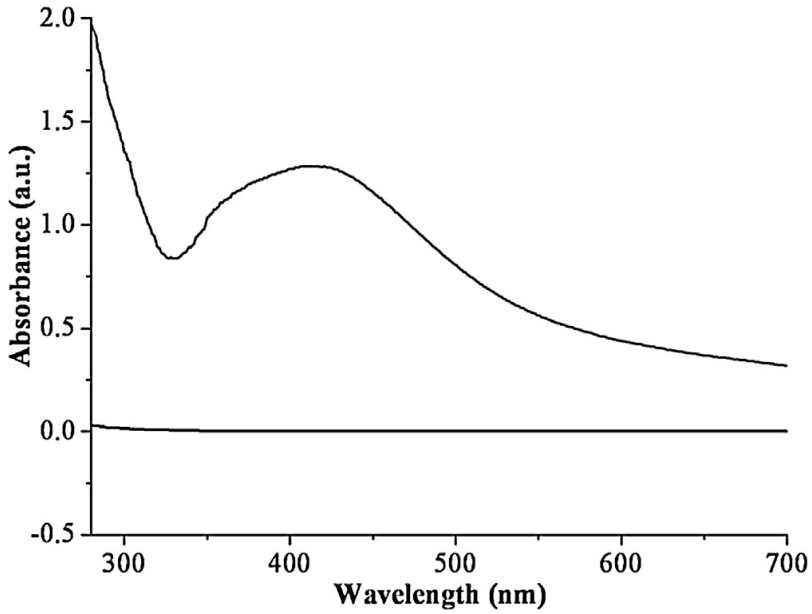

Figure 7. Diffuse reflectance UV–vis spectra of AgNPs loaded on PM fibres (black solid line) and AgNPs loaded on PPAA coated PM fibres (grey solid line).

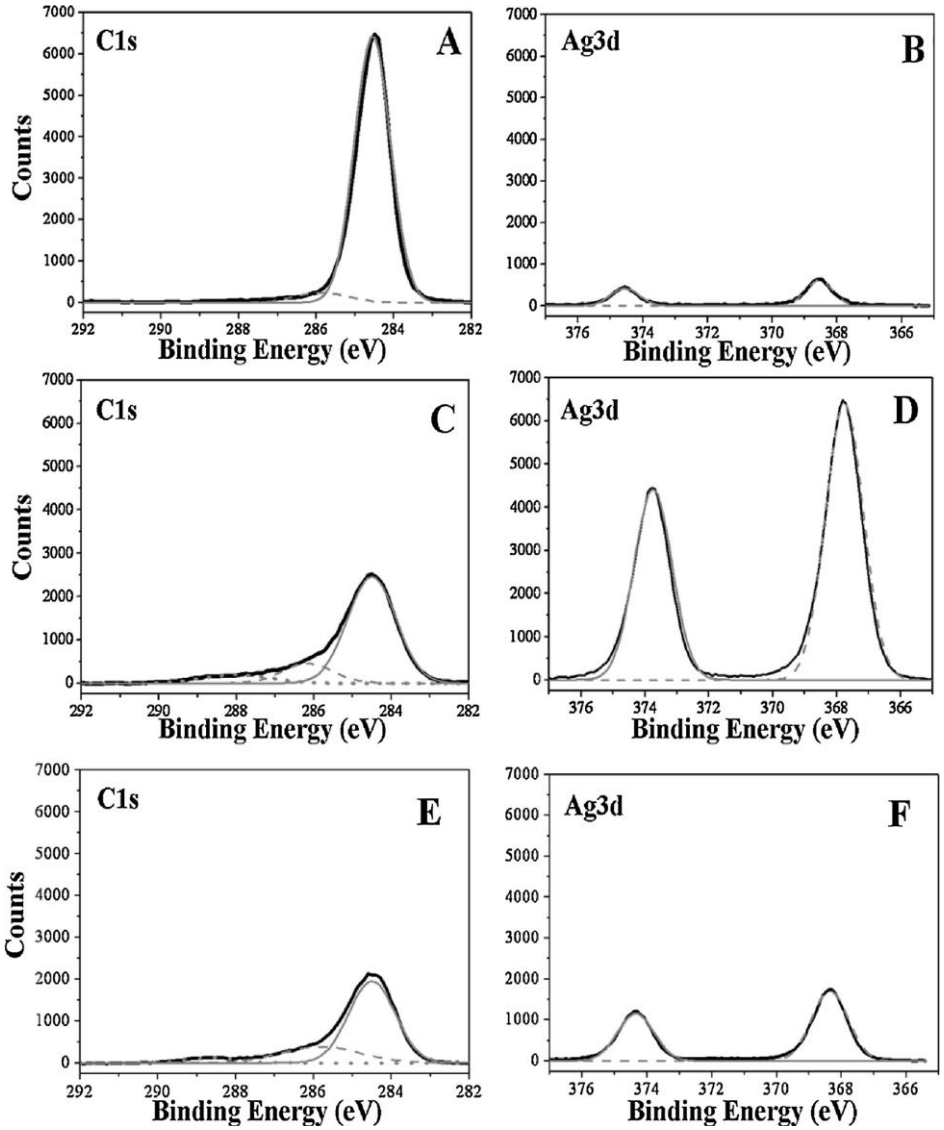

Figure 8. XPS spectra of: (i) AgNPs loaded on PM fibres: C1s signal (A) and Ag3d signal (B); (ii) AgNPs loaded on PPAA coated PM fibres: C1s signal (C) and Ag3d signal (D); (iii) AgNPs loaded on PPAA coated PP/ePTFE meshes: C1s signal (E) and Ag3d signal (F). C1s signals: experimental curve (black solid line), C–C/C–H signal at 284.5 eV (grey solid line), C–O signal at 286.0 eV (grey dashed line) and HO–C=O signal at 287.9 eV (grey dotted line). Ag3d signals: experimental curve (black solid line), $Ag^0 3d^{3/2}$ at 374 eV (grey solid line) and $Ag^0 3d_{5/2}$ at 368.5 eV (grey dashed line).

Table 1. Average carboxyl functionality density evaluated for PP and PP/ePTFE samples.

Samples name	Carboxyl functionality density[a)]
PM before functionalisation	0
PPAA functionalised PM (geometrical area)	$(6.32 \pm 3.45) \times 10^{13}$
AM not treated	0
PPAA functionalised AM	$(7.68 \pm 1.82) \times 10^{14}$

a) Carboxylic functionality densities are reported in number of –COOH groups per cm^2 of mesh ± SD (or standard deviation).

Table 2. Results of preliminary ICP-AES tests concerning Ag loading (before and after water soaking) and Ag release in water for PM samples.

Samples name	Ag amount (mg)[a)]	[Ag] (wt.%)[b)]
AgNPs on PPAA coated PM	0.311	1.1
AgNPs on PPAA coated PM after release in water	0.239	0.9
AgNPs measured in soaking water	0.040	0.1

a) The Ag amount is reported as mg of Ag released by 9 cm^2 of mesh after 15 days soaking in water.
b) The [Ag] weight ratio is calculated as the % between ICP-AES measured Ag amount and the weight of 9 cm^2 of PP mesh (from the mesh grammage: 27 mg).